



Cite this: DOI: 10.1039/d5fb00922g

# Optimised ultrasound treatments enhance hydration properties and induce structural modifications in dietary fibre concentrates derived from orange peels

Julia Nutter,<sup>ab</sup> Robert Soliva-Fortuny,<sup>ab</sup> Olga Martín-Belloso<sup>ab</sup>  
and Pedro Elez-Martínez<sup>ab\*</sup>

Recent studies have focused on the modification of individual soluble and insoluble dietary fibre (DF) fractions from fruit by-products to enhance the techno-functional properties of ingredients. However, the potential to improve these properties in DF concentrates while preserving the combined functionality of both fractions remains underexplored. This study aimed to optimise ultrasound treatment conditions—power (W), solid–liquid ratio (g mL<sup>-1</sup>), and time (min)—to improve the hydration properties of DF concentrates derived from orange peels (OP-DFC) and to explore the structure–function relationships associated with ultrasound-induced modifications. Ultrasound treatments resulted in the selective enhancement of solubility (SOL, 320 W, 1:30 g mL<sup>-1</sup>, 30 min), swelling capacity (SC, 80 W, 1:25 g mL<sup>-1</sup>, 25.6 min), and water retention capacity (WRC, 208 W, 1:20 g mL<sup>-1</sup>, 30 min), with increases of up to 60% compared with untreated OP-DFC. Simultaneous optimisation yielded the best compromise at 188 W, 1:28 g mL<sup>-1</sup>, and 30 min. Enhancements in hydration properties were associated with cavitation-induced structural modifications, including matrix disruption, increased porosity, and partial depolymerisation of DF. These changes were reflected in a decrease in the insoluble DF content from 49.4% to 42.4–46.2% and an increase in the soluble DF content from 6.6% to 9.5–12.1%. From a technological perspective, increased SOL facilitates ingredient incorporation into foods while higher SC and WRC enhance rehydration behaviour and binder performance across a wide range of products. Overall, this strategy supports the development of clean-label, DF-rich ingredients from orange by-products with targeted hydration functionalities, broadening their potential use in diverse formulations.

Received 27th November 2025

Accepted 24th April 2026

DOI: 10.1039/d5fb00922g

rsc.li/susfoodtech

## Sustainability spotlight

During orange processing for juice production, the food industry generates large amounts of pulp and peels that are typically discarded despite their potential as cost-effective sources of dietary fibre. This study demonstrated that, by optimising treatment conditions, ultrasound processing can be strategically applied to tailor the hydration properties of orange-peel dietary fibre concentrates, enhancing their potential use in food formulations. This work aligns with the UN's Sustainable Development Goals 12, 9, and 3 by promoting the valorisation of underutilised biomass, the adoption of energy-efficient processing technologies, and the development of fibre-enriched ingredients that support healthier diets.

## 1. Introduction

The growing consumer interest in healthy, clean-label ingredients produced through more sustainable processes has driven the food industry to adopt innovative approaches that align with these demands.<sup>1</sup> In this context, the development of novel dietary fibre (DF)-rich ingredients is particularly relevant given the well-documented physiological benefits of DF, including cholesterol reduction, attenuation of glycaemic response, and improvements in gut and metabolic health.<sup>2</sup>

Fruit transformation industries generate large volumes of underutilised by-products that represent cost-effective sources of DF. Orange peel is especially attractive due to its abundance and high levels of DF, with relatively high proportions of soluble DF (SDF), mainly pectin.<sup>3</sup> The balance between SDF and insoluble DF (IDF) largely determines the performance of DF-rich ingredients once incorporated into foods. On the one hand, soluble fractions disperse easily in aqueous systems, facilitating their integration into diverse formulations, although high levels of pectin may cause undesirable viscosity increases in liquid and certain semi-solid products.<sup>4,5</sup> On the other hand, insoluble fractions contribute to water retention capacity (WRC),<sup>6–8</sup> which can improve juiciness in processed meats and meat analogues<sup>8,9</sup> and storage stability in baked goods.<sup>10</sup> However, DF competes

<sup>a</sup>Department of Food Technology, Engineering, and Science, University of Lleida, Rovira Roure Ave, 191, Lleida, E25198, Spain. E-mail: pedro.elez@udl.cat

<sup>b</sup>Agrotecnio Research Centre, CERCA, Rovira Roure Ave, 191, Lleida, E25198, Spain



with other food constituents for water molecules, interfering with gluten development and starch gelatinization and, thus, leading to final products of lower sensory acceptance.<sup>11,12</sup> In this context, evaluating hydration properties, such as solubility (SOL), water retention capacity (WRC), and swelling capacity (SC) provides an initial indication of how a novel ingredient may behave when incorporated into foods.<sup>6</sup>

The technological limitations associated with SDF and IDF highlight the need for innovative processing strategies capable of modulating DF fractions and enhancing their techno-functional performance. Traditionally, physical, chemical, thermal, and enzymatic methods have been used, individually or combined, to extract DF fractions or isolate specific polysaccharides from fruit by-products.<sup>1</sup> More recently, research efforts have been focused on modifying the fibre composition and structure rather than isolating specific fractions.<sup>13–16</sup> This approach aims to preserve and even enhance the combined physiological and techno-functional benefits of IDF and SDF within a single product,<sup>1</sup> while reducing the processing steps associated with purification and isolation.

Ultrasound (US) is recognised as a “green” physical processing technology, as it can be operated at mild temperatures and under water-based processes, minimising or avoiding the use of chemical reagents, while requiring relatively short processing times and low energy inputs.<sup>17,18</sup> In US, soundwaves generate positive and negative pressure cycles in a liquid medium. When the negative pressure exceeds the medium’s tensile strength, bubbles form, expand, and collapse. The violent collapse near solid surfaces creates high velocity microjets that can rupture plant tissues and loosen cell wall polymer networks.<sup>15</sup> However, research on US modification of DF derived from orange by-products remains limited. Among these, most studies focus on the modification of isolated DF fractions or polysaccharides,<sup>6,7,19–22</sup> which may increase process complexity and do not fully exploit the combined functionality of both SDF and IDF fractions. In contrast, novel ingredients obtained through physical modification of DFC could benefit from the hydration properties of both DF fractions simultaneously. To the best of our knowledge, only one study has evaluated the effect of US treatment on orange by-products to modify their techno-functional and physiological properties.<sup>23</sup> In that study, only modest improvements in WHC and no enhancement in SOL were reported for powders derived from orange pulp and peel mixtures, highlighting the need to explore a broader range of processing conditions and optimisation strategies. Therefore, the present study aimed to evaluate and optimise the effect of US treatment conditions (power, solid-liquid ratio, and time) to improve the hydration properties of DF concentrates derived from orange peel (OP-DFC). Additionally, it sought to explore the structure–function relationships underlying potential modifications induced by US.

## 2. Materials and methods

### 2.1. Materials

Oranges (*Citrus sinensis* var. Navel) at edible maturity stage (total soluble solids: 11.9 °Brix, acidity: 1.1% citric acid) were

acquired from a local market (Lleida, Spain). Ascorbic acid, citric acid, pepsin (695 IU per mg), and  $\alpha$ -amylase (13 IU per mg) were provided by Sigma-Aldrich (Saint Louis, Missouri, USA), and amyloglucosidase (14 IU per mg) was acquired from Roche (Basel, Switzerland).

### 2.2. Obtention of dietary fibre concentrates from orange peels

Oranges [78.53  $\pm$  0.59% moisture, 60.08  $\pm$  0.70% (dry weight basis, dw) total dietary fibre (TDF), 26.28  $\pm$  0.32% (dw) digestible carbohydrates, 5.73  $\pm$  0.19% (dw) protein, 4.52  $\pm$  0.30% (dw) fat, and 3.02  $\pm$  0.17% (dw) ash] were decontaminated with sodium hypochlorite (135 mM), rinsed, dried, and peeled. The peels were chopped and washed sequentially with hot deionized water (85 °C), cold deionized water (4 °C), a citric acid (5 g L<sup>-1</sup>)-ascorbic acid (10 g L<sup>-1</sup>) solution, and deionized water at room temperature to reduce potential enzymatic activity.<sup>16</sup> The peels were drained, freeze-dried (–80 °C, 0.6 mbar, 96 h), ground, sieved (<0.2 mm), packed in hermetic polyethylene containers, and stored at –40 °C. The moisture content of the resulting OP-DFC was 9.06  $\pm$  0.15%.

### 2.3. Experimental design

A three-factor, three-level Box–Behnken design with 15 experimental runs, including three central points, was used to investigate the effects of US power ( $X_1$ ), solid–liquid ratio (SLR,  $X_2$ ), and treatment time ( $X_3$ ) on the hydration properties (SOL, SC, and WRC) of OP-DFC (Table 1). Power was evaluated at 80, 200, and 320 W; SLR at 1:30, 1:25, and 1:20 g mL<sup>-1</sup>; and treatment time at 10, 20, and 30 min. Selected power levels and treatment times were within the ranges reported in literature to allow structural modification and prevent excessive polysaccharide degradation in similar DF-rich matrices, whereas the SLR range was selected to ensure proper contact between the solvent and OP-DFC and to avoid excessive viscosity of the suspension, which may hinder cavitation efficiency.<sup>15</sup> The experimental runs were performed in random order. A second-order polynomial model (eqn (1)) was fitted to the data using the least squares regression method, where  $Y$  is the predicted response (SOL, SC, WRC),  $X_i$ ,  $X_iX_j$ , and  $X_i^2$  are the linear, interaction, and quadratic effects of the independent variables influencing the response variables, respectively, and  $\beta_0$ ,  $\beta_i$ ,  $\beta_{ij}$ , and  $\beta_{ii}$  are the regression coefficients for the intercept, linear, interaction, and quadratic terms, respectively.

$$Y = \beta_0 + \sum_{i=1}^3 \beta_i X_i + \sum_{i=1}^2 \sum_{j=2, j>i}^3 \beta_{ij} X_i X_j + \sum_{i=1}^3 \beta_{ii} X_i X_i^2 \quad (1)$$

Response surface methodology (RSM) was used to determine the best conditions for maximising the response variables, individually and simultaneously, with the desirability function under the larger-the-best criterion.<sup>24</sup> Each model was validated by performing a set of three independent experiments using the conditions obtained from the individual and simultaneous optimisations to evaluate the reliability of the predicted models.



Table 1 Box–Behnken design for ultrasound treatment conditions and their response variables expressed as mean  $\pm$  standard deviation ( $N = 3$ )<sup>a</sup>

Run	Independent variables			Response variables			
	Power ( $X_1$ , W)	Solid–liquid ratio ( $X_2$ , g mL <sup>-1</sup> )	Time ( $X_3$ , min)	Solubility (% dw)	Swelling capacity (mL g <sup>-1</sup> dw)	Water retention capacity (g g <sup>-1</sup> dw)	Total energy input (kJ kg <sup>-1</sup> )
1	80	1 : 30	20	48.45 $\pm$ 1.35	15.95 $\pm$ 0.71	6.57 $\pm$ 0.35	240
2	80	1 : 20	20	40.20 $\pm$ 2.36	15.65 $\pm$ 0.81	6.72 $\pm$ 0.17	240
3	320	1 : 30	20	56.87 $\pm$ 2.03	12.12 $\pm$ 0.53	6.28 $\pm$ 0.64	960
4	320	1 : 20	20	52.08 $\pm$ 2.07	12.51 $\pm$ 0.51	7.09 $\pm$ 0.18	960
5	80	1 : 25	10	40.67 $\pm$ 2.30	15.46 $\pm$ 0.80	6.36 $\pm$ 0.03	120
6	80	1 : 25	30	45.01 $\pm$ 0.36	17.28 $\pm$ 0.90	7.13 $\pm$ 0.38	360
7	320	1 : 25	10	45.79 $\pm$ 1.52	13.90 $\pm$ 0.13	6.37 $\pm$ 0.47	480
8	320	1 : 25	30	57.12 $\pm$ 2.31	10.48 $\pm$ 0.50	7.90 $\pm$ 0.19	1440
9	200	1 : 30	10	44.76 $\pm$ 1.74	14.45 $\pm$ 0.23	7.34 $\pm$ 0.34	300
10	200	1 : 30	30	54.23 $\pm$ 3.01	13.47 $\pm$ 0.31	8.02 $\pm$ 0.27	900
11	200	1 : 20	10	41.43 $\pm$ 1.57	14.35 $\pm$ 0.42	6.85 $\pm$ 0.35	300
12	200	1 : 20	30	47.97 $\pm$ 2.35	13.42 $\pm$ 0.33	8.72 $\pm$ 0.35	900
13	200	1 : 25	20	46.90 $\pm$ 1.16	15.39 $\pm$ 0.32	7.92 $\pm$ 0.43	600
14	200	1 : 25	20	46.44 $\pm$ 1.16	15.62 $\pm$ 0.59	7.55 $\pm$ 0.19	600
15	200	1 : 25	20	47.49 $\pm$ 1.04	16.04 $\pm$ 0.51	7.55 $\pm$ 0.29	600
UT-1 : 30	0	1 : 30	0	40.82 $\pm$ 1.09	10.95 $\pm$ 0.28	6.19 $\pm$ 0.04	0
UT-1 : 25	0	1 : 25	0	40.36 $\pm$ 1.41	10.84 $\pm$ 0.42	6.28 $\pm$ 0.31	0
UT-1 : 20	0	1 : 20	0	40.32 $\pm$ 2.12	10.63 $\pm$ 0.12	6.31 $\pm$ 0.19	0

<sup>a</sup> UT-1 : 30, UT-1 : 25, and UT-1 : 20 refer to untreated dietary fibre concentrates derived from orange peels (OP-DFC) prepared at solid–liquid ratios of 1 : 30, 1 : 25, and 1 : 20, respectively, to match the conditions used for the ultrasound-treated OP-DFC.

The relative standard error (RSE) was calculated for each pair of predicted and experimental values (eqn (2)). An RSE below a 10% was considered acceptable. The conditions resulting in the maximum SOL, SC, and WRC were coded as SOL-OPT, SC-OPT, and WRC-OPT, respectively, meanwhile that resulting from the simultaneous optimisation was coded as SIM-OPT. OP-DFC obtained under optimal conditions were subsequently characterised.

Relative standard error

$$= \frac{|\text{predicted value} - \text{experimental value}|}{\text{predicted value}} \times 100 \quad (2)$$

## 2.4. Ultrasound treatments

Ultrasound treatments were performed using an UP400S ultrasonic homogenizer (Hielscher Ultrasonics GmbH, Teltow, Germany) operating at a frequency of 24 kHz and a maximum nominal power output of 400 W (100% amplitude), equipped with a 14 mm diameter sonotrode (maximum amplitude of 125  $\mu$ m, H14, Hielscher Ultrasonics GmbH, Teltow, Germany). The device amplitude was adjusted to 20, 50, and 80% to deliver US powers of 80, 200, and 320 W, respectively. OP-DFC was dispersed in distilled water (suspension mass of 200 g), stirred at 1000 rpm for 30 min, stored at 4  $^{\circ}$ C for 1 h, and then transferred into a double-jacketed sample vessel with water recirculation (4  $^{\circ}$ C) and constant stirring (500 rpm). The sonotrode tip was immersed in the suspension, leaving a 4 cm gap between the tip and the vessel bottom. OP-DFC suspensions were treated in pulsed mode (50% duty cycle, 1 s on, 1 s off) under the conditions specified in Table 1. Ultrasound power, treatment time, duty cycle, and the mass of OP-DFC suspensions were

used to calculate the total energy input (eqn (3)). Untreated OP-DFC suspensions were prepared at 1 : 30, 1 : 25, and 1 : 20 SLR as control. Untreated and US-treated suspensions were immediately freeze-dried ( $-80$   $^{\circ}$ C, 0.6 mbar, 96 h), sieved ( $<0.2$  mm), and stored in hermetic polyethylene containers at  $-40$   $^{\circ}$ C for subsequent analysis.

$$\begin{aligned} \text{Total energy input (E, J kg}^{-1}\text{)} \\ = \frac{\text{power(W)} \times [0.5 \times \text{time (s)}]}{\text{OP-DFC suspension mass(kg)}} \end{aligned} \quad (3)$$

## 2.5. Techno-functional properties

The hydration properties (SOL, SC, and WRC) and the oil retention capacity (ORC) were evaluated following the procedures described by Nutter *et al.* (2025)<sup>14</sup> and calculated from eqn (4)–(7), respectively. Solubility describes the fraction of DF that dissolves in water, SC reflects the ability of the DF matrix to absorb water expand, and WRC and ORC represent the capacity of the DF matrix to physically entrap water or oil, respectively. Results were expressed on a dw basis.

$$\text{SOL}(\%, \text{ dw}) = \frac{W_{\text{OP-DFC}} - W_{\text{DP}}}{W_{\text{OP-DFC}}} \times 100 \quad (4)$$

$$\text{SC}(\text{mL g}^{-1}, \text{ dw}) = \frac{V_{\text{P}}}{W_{\text{OP-DFC}}} \quad (5)$$

$$\text{WRC}(\text{g g}^{-1}, \text{ dw}) = \frac{W_{\text{W}}}{W_{\text{OP-DFC}}} \quad (6)$$

$$\text{ORC}(\text{g g}^{-1}, \text{ dw}) = \frac{W_{\text{O}}}{W_{\text{OP-DFC}}} \quad (7)$$



where  $W_{OP-DFC}$  is the weight of OP-DFC;  $W_{DP}$  is the weight of the pellet resulting from OP-DFC after solubilisation in excess water (3 h), centrifugation, and drying (60 °C, 24 h);  $V_p$  is the volume occupied by the hydrated OP-DFC after incubation in excess water for 24 h;  $W_w$  and  $W_o$  are the weights of water or oil adsorbed by the pellet resulting from OP-DFC after incubation in excess water (24 h) or oil (1 h), respectively.

## 2.6. Physical properties

The apparent viscosity of 6% (w/w) OP-DFC suspensions was measured using an SV-10 vibro-viscosimeter (A&D Instruments Ltd, Abingdon, UK) at 25 °C and after 24 h of storage at 4 °C. This concentration was selected to comply with the “source of fibre” claim (>3% TDF) by the European Safety Authority (EFSA),<sup>25</sup> based on the TDF content in OP-DFC (2.2). The mean particle size was determined by laser diffraction using a MS3000 mastersizer (Malvern Instrument, Worcestershire, UK). Orange peel-DFC were dispersed in deionized water (1% w/v) and transferred into the instrument’s dispersion unit. The mean particle size, defined as the diameter (in  $\mu\text{m}$ ) at which 50% of the particle volume is smaller and 50% is larger, was calculated by the instrument software from the particle size distribution curve.

## 2.7. Total, insoluble and soluble dietary fibre content

The DF content was determined using the gravimetric–enzymatic method described by Goñi *et al.* (2009).<sup>26</sup> Briefly, OP-DFC (300 mg) was dispersed in 10 mL phosphate buffer (0.1 M, pH 7.5), the pH was adjusted to 1.5, and the suspension was incubated at 40 °C for 1 h with 0.2 mL pepsin solution (300 mg mL<sup>-1</sup>, in 0.08 M HCl-KCl). The pH was raised to 7.5, and the suspension was incubated at 37 °C for 6 h with 1 mL pancreatin solution (5 mg mL<sup>-1</sup>, in 0.1 M phosphate buffer). Subsequently, 10 mL of phosphate buffer (pH 7.5) was added, the pH adjusted to 6.9, and the suspension incubated at 37 °C for 16 h with 1 mL  $\alpha$ -amylase solution (162 mg mL<sup>-1</sup>, in 0.1 M trizma-maleate buffer). The enzymatic hydrolysate was centrifuged (3000 $\times$ g, 15 min, 4 °C), and the pellet washed twice and dried at 105 °C for 24 h to obtain the IDF fraction. Sodium acetate buffer (0.2 M, 10 mL, pH 4.75) was added to the supernatant and incubated (60 °C, 45 min) with 0.1 mL amyloglucosidase solution (10 mg mL<sup>-1</sup>). The supernatant was dialysed (12 kDa cut-off cellulose membranes) for 48 h, and the dialysate was freeze-dried (–80 °C, 0.6 mbar, 96 h) to yield the SDF fraction. TDF was calculated as the sum of IDF and SDF. An enzyme blank was subtracted from both IDF and SDF fractions. Results were expressed as grams per 100 g (% dw).

## 2.8. Microstructure

The microstructure was examined by scanning electron microscopy (SEM). Briefly, OP-DFC were placed on double-sided carbon tape, coated with a thin layer of gold (90 s, 30 mA), and visualized with an FEI Scios DualBeam scanning electron microscope (Fei Company, Hillsboro, Oregon, USA) operating at an accelerating voltage of 20 kV. Images were obtained at magnifications of 300, 1000, and 5000-fold.

## 2.9. Thermal properties

The thermal analysis was evaluated by differential scanning calorimetry (DSC) using a STARE SYSTEM DSC 3+ differential scanning calorimeter (Mettler Toledo, Columbus, OH, USA). For this purpose, 4–6 mg of OP-DFC was transferred into 40- $\mu\text{L}$  aluminium crucibles, and the experiments were conducted in an inert N<sub>2</sub> atmosphere (50 mL per min flow). The temperature range was 30–200 °C and the heating rate was 10 °C min<sup>-1</sup>. The peak temperature was acquired from the thermograms using STARE Excellence software (Mettler Toledo, Columbus, Ohio, USA).

## 2.10. Crystalline structure

The crystalline structure was analysed by X-ray diffraction (XRD) using an Ru2500 Rigaku diffractometer (Rigaku, Neu-Isenburg, Germany) equipped with a rotating anode. The instrument was operated at 40 kV and 80 mA with a Cu anode, and a graphite monochromator was used to select the K $\alpha$  radiation. Diffraction patterns were recorded over a diffraction angle ( $2\theta$ ) of 10° to 50°, with a step size of 0.03° and, 1 s per step.

## 2.11. Molecular structure

The molecular structure was studied by Fourier transform infrared (FTIR) spectroscopy. Measurements were performed on a 6300 FT-IR spectrometer (Jasco Inc., Madrid, Spain) equipped with a MIRacle attenuated total reflectance accessory (Pike Technologies, Madison, Wisconsin, USA). Spectra were recorded in absorbance mode by averaging 32 scans over the range of 4000–650 cm<sup>-1</sup>, with a resolution of 4 cm<sup>-1</sup>. A background spectrum was acquired prior to each measurement to account for environmental variations. Spectra were baseline-corrected and normalized to minimise confounding effects such as sample thickness.<sup>27</sup> Normalization to the C–H stretching vibration band ( $\sim$ 2930 cm<sup>-1</sup>) was performed due its stability across samples and lack of overlap with other bands.

## 2.12. Statistical analysis

Experimental runs (Table 1) were performed in triplicate; three independently prepared suspensions were subjected to the same treatment conditions. Results were reported as mean  $\pm$  standard deviation. Data was analysed using JMP version 18.0.1 (JMP Statistical Discovery LLC, Cary, North Carolina, USA). For RSM, analysis of variance (ANOVA) followed by Tukey’s multiple comparison test was performed. Model adequacy was assessed through lack of fit tests, coefficient of determination ( $R^2$ ), and adjusted  $R^2$  using a 95% confidence level. Comparisons between optimal treatments were also performed using ANOVA followed by Tukey’s test.

# 3. Results & discussion

## 3.1. Effect of ultrasound treatment conditions and process optimisation

Response surface methodology using a Box–Behnken experimental design was employed to evaluate the effects of US



**Table 2** Estimated regression coefficients of the adjusted quadratic models obtained for solubility (SOL), swelling capacity (SC), and water retention capacity (WRC) with response surface methodology as a function of coded variables for power ( $X_1$ ), solid-liquid ratio ( $X_2$ ), and time ( $X_3$ )<sup>a</sup>

	SOL (%)			SC (mL g <sup>-1</sup> )			WRC (g g <sup>-1</sup> )		
	Parameter estimates	Standard error	<i>p</i> -value	Parameter estimates	Standard error	<i>p</i> -value	Parameter estimates	Standard error	<i>p</i> -value
Intercept	46.2805	0.5362	<0.0001**	15.6822	0.1814	<0.0001**	7.7061	0.0814	<0.0001**
Linear							—	—	NS
$X_1$	4.6929	0.3947	<0.0001**	-1.9138	0.1111	<0.0001**	—	—	NS
$X_2$	-2.8542	0.3947	<0.0001**	—	—	NS	—	—	—
$X_3$	3.9854	0.3947	<0.0001**	-0.4350	0.1111	0.0004**	0.6142	0.0762	<0.0001**
Crossed									
$X_1 X_2$	—	—	NS	—	—	NS	—	—	NS
$X_1 X_3$	1.7501	0.5581	0.0033**	-1.3033	0.1571	<0.0001**	—	—	NS
$X_2 X_3$	—	—	NS	—	—	NS	0.2975	0.1077	<0.0001**
Quadratic									
$X_1^2$	1.3641	0.5792	0.0238*	-0.6290	0.1635	0.0005**	—	—	NS
$X_2^2$	1.2616	0.5792	0.0357*	-0.9907	0.1635	<0.0001**	-0.8954	0.1115	<0.0001**
$X_3^2$	—	—	NS	-0.7732	0.1635	<0.0001**	—	—	NS
Lack of fit	0.1443			0.5907			0.1030		
ANOVA	<0.0001**			<0.0001**			<0.0001**		
$R^2$	0.8924			0.9233			0.7853		
$R^2$ adjusted	0.8753			0.9088			0.7578		
Desirability	0.996			0.864			0.864		

<sup>a</sup> Coefficients with *p*-values between 0.01 and 0.05 and less than 0.01 were considered significant (\*) and highly significant (\*\*), respectively. Coefficients with *p*-values greater than 0.05 were considered not significant (NS) and were excluded from the final models (—).

treatment conditions, namely power, SLR, and treatment time, on the hydration properties of OP-DFC. Table 1 summarizes the experimental design and the corresponding values of SOL, SC, and WRC, whereas Table 2 shows the regression coefficients of the adjusted quadratic models obtained for these response variables. The associated RSM plots are presented in Fig. I–III of the SI.

Solubility increased at most US treatment conditions (Table 1). The highest SOL was attained at 320 W, 1 : 30 SLR, and 30 min (1440 kJ kg<sup>-1</sup>), representing a 40% increase compared with the untreated OP-DFC. The ANOVA ( $p < 0.0001$ , adjusted  $R^2$  0.88) confirmed that the quadratic model adequately fitted the experimental data, allowing reliable prediction of SOL.

Solubility increased ( $p < 0.0001$ ) with both power ( $X_1$ ) and treatment time ( $X_3$ ), and their interaction ( $X_1 X_3$ ) was also significant ( $p = 0.0033$ ), indicating a synergistic effect. Increasing the applied power intensifies the acoustic energy delivered to the medium, causing cavitation bubbles to form and collapse more violently near plant tissue surfaces and generating intense microjets and shear forces that fragment cell walls.<sup>15,18</sup> This structural disruption facilitates the release of soluble constituents, including SDF, sugars, proteins, and bioactive compounds,<sup>28–30</sup> as well as the weakening of inter- and intramolecular non-covalent bonds within the DF network, increasing the availability of hydrophilic groups for water interaction.<sup>16,31</sup> These effects are further accentuated as treatment time progresses,<sup>15</sup> ultimately leading to the observed rise in OP-DFC SOL. Furthermore, SOL increased ( $p < 0.0001$ ) as SLR ( $X_2$ ) decreased from 1 : 20 to 1 : 30 g mL<sup>-1</sup>, meaning that US-induced solubilisation was favoured in more diluted OP-DFC suspensions. Lower SLR enhances mass transfer by increasing the contact area between the solvent and plant material,

promoting the release and dissolution of soluble polysaccharides.<sup>32</sup> Additionally, at lower SLR (e.g., 1 : 30), less solid material is available to absorb the acoustic energy, which may intensify matrix disruption and further increase the exposure of hydrophilic groups, thereby promoting solubilisation. In contrast, cavitation is typically attenuated in more concentrated suspensions (e.g., 1 : 20) because bubble formation requires greater energy to overcome the strong cohesive forces characteristic of viscous liquids.<sup>33</sup>

The quadratic terms for power ( $X_1^2$ ) and SLR ( $X_2^2$ ) were significant ( $p < 0.05$ ) and positive, suggesting that SOL increased more sharply at higher powers, whereas the effect of SLR was more attenuated between high-to-intermediate ratios (1 : 20–1 : 25) but became more pronounced when moving from intermediate-to-low ratios (1 : 25–1 : 30).

Swelling capacity increased by up to 60% following US treatments respect to untreated OP-DFC (Table 1), with the highest value obtained at 80 W, 1 : 25 SLR, and 30 min (360 kJ kg<sup>-1</sup>). The experimental data were well fitted by the quadratic model ( $p < 0.0001$ , adjusted  $R^2$  0.91), supporting a reliable prediction of the response. Power ( $X_1$ ) had a significant ( $p < 0.0001$ ) negative effect on SC, meaning that lower powers enhanced the ability of OP-DFC to absorb water and expand, but this effect was attenuated as power increased from 80 to 320 W. Similarly, treatment time ( $X_3$ ) exerted a significant ( $p = 0.0004$ ) negative effect, with higher SC values observed at shorter sonication times. The interaction between power and time was also significant and negative ( $p < 0.0001$ ), suggesting that applying low powers for short periods further enhanced the SC of OP-DFC. Additionally, all quadratic terms were significant ( $p < 0.001$ ) and negative, indicating that SC would generally peak at intermediate levels of the factors. The



swelling of plant cell wall polysaccharides results from a balance between hydration forces, driven by the interaction of water with hydrophilic groups, and elastic resistance exerted by ionic and covalent bonds within the DF network. In this context, US can disrupt intra- and intermolecular interactions and consequently expose additional hydroxyl groups, therefore increasing the driving forces for matrix swelling.<sup>33</sup> Moderate-intensity and relatively short treatments may open small pores in the matrix,<sup>34</sup> shifting the equilibrium towards water-polymer interactions. In contrast, high-intensity and prolonged treatments likely cause structural collapse, thus reducing the swelling capacity of OP-DFC.

Water retention capacity increased under certain US conditions, reaching a peak at 200 W, 1 : 20 SLR, and 30 min (900 kJ kg<sup>-1</sup>), corresponding to a 40% increase compared with untreated OP-DFC. The predicted quadratic model showed an acceptable fit to the experimental data ( $p < 0.0001$ , adjusted  $R^2$  0.76), allowing a reasonably reliable prediction of the response. Treatment time ( $X_3$ ) had a significant ( $p < 0.0001$ ) positive effect, indicating that longer sonication favoured the ability of OP-DFC to adsorb water. The interaction between SLR and treatment time ( $X_2X_3$ ) was also significant ( $p < 0.0001$ ) and positive, indicating that at more concentrated OP-DFC suspensions, longer US exposure further increased the WRC. Moreover, the quadratic term for SLR was significant ( $p < 0.01$ ) and negative, meaning that WRC peaked at intermediate-to-high concentrations. Water retention capacity arises from both the physical entrapment of water within a porous matrix and the adsorption of water molecules onto hydrophilic groups. Ultrasound disrupts the DF network creating pores and microchannels that enhance water binding by capillary effects while increasing the availability of hydrophilic groups through surface area enlargement.<sup>34,35</sup> In this context, longer treatments might promote progressive structural reorganisation of the DF network, while more concentrated suspensions favour a controlled distribution of acoustic energy. This combination possibly limits excessive matrix collapse<sup>33</sup> and instead improves the matrix's ability to adsorb and entrap water, ultimately increasing its WRC.

The optimal conditions that maximised the hydration properties of OP-DFC are presented in Table 3. For individual responses, maximum values were predicted at 320 W, 1 : 30 SLR, 30 min for SOL, 80 W, 1 : 25 SLR, 25.6 min for SC, and 208 W, 1 : 20 SLR, 30 min for WRC, whereas simultaneous optimization yielded the best compromise at 188 W, 1 : 28 SLR, and 30 min treatment time. Overall, the validation of the models showed close agreement between predicted and experimental values, with RSE below 10% generally considered acceptable. For simultaneous optimization, the RSE for WRC was slightly higher but remained acceptable given the multi-response compromise.

### 3.2. Characterisation of OP-DFC treated under optimal US conditions

The US treatment conditions that maximised SOL, SC, and WRC of OP-DFC are hereafter referred to as SOL-OPT (320 W, 1 : 30 SLR, 30 min, 1440 kJ kg<sup>-1</sup>), SC-OPT (80 W, 1 : 25 SLR, 25.6 min, 307 kJ kg<sup>-1</sup>), and WRC-OPT (208 W, 1 : 20 SLR, 30 min, 936 kJ kg<sup>-1</sup>), respectively, whereas the condition corresponding to the simultaneous optimisation is referred to as SIM-OPT (188 W, 1 : 28 SLR, 30 min, 846 kJ kg<sup>-1</sup>). The appearance of the OP-DFC obtained under these conditions is shown in Fig. IV of the SI. Ultrasound-treated OP-DFC were subsequently characterised in their techno-functional and physical properties, DF content, microstructure, crystalline structure, thermal properties, and molecular structure.

**3.2.1. Techno-functional properties.** As previously discussed (3.1), US treatments led to a general enhancement in the hydration properties of OP-DFC, regardless of the optimisation conditions applied (Fig. 1A). SOL increased by 54, 38, 31, and 24% in OP-DFC treated under SOL-OPT, SIM-OPT, WRC-OPT, and SC-OPT, respectively, compared with untreated OP-DFC. As expected, higher powers and longer treatment time resulted in higher OP-DFC solubilisation. Moreover, when comparing treatments with similar powers (*i.e.*, WRC-OPT and

**Table 3** Individual and simultaneous optimisation of ultrasound treatment conditions to maximise the solubility (SOL), swelling capacity (SC), and water retention capacity (WRC) of dietary fibre concentrates derived from orange peels (OP-DFC), with predicted and experimental responses under these conditions<sup>a</sup>

		Optimised condition				Response		
		Power (W)	SLR (g mL <sup>-1</sup> )	Time (min)	Total energy input (kJ kg <sup>-1</sup> )	Predicted	Experimental	RSE (%)
Individual optimization	SOL	320	1 : 30	30	1440	62.19%	62.82 ± 2.35%	1.0
	SC	80	1 : 25	25.6	307	17.21 mL g <sup>-1</sup>	16.12 ± 0.28 mL g <sup>-1</sup>	6.7
	WRC	208	1 : 20	30	936	8.77 g g <sup>-1</sup>	8.74 ± 0.06 g g <sup>-1</sup>	0.3
Simultaneous optimization		188	1 : 28	30	846	SOL = 50.80%	SOL = 56.32 ± 0.73%	9.8
						SC = 14.59 mL g <sup>-1</sup>	SC = 12.85 ± 0.58 mL g <sup>-1</sup>	13.5
						WRC = 8.32 g g <sup>-1</sup>	WRC = 8.06 ± 0.14 g g <sup>-1</sup>	3.2
Untreated	0	1 : 25*	0	0		SOL = 40.90 ± 1.74%		
						SC = 10.77 ± 5.12 mL g <sup>-1</sup>		
						WRC = 6.42 ± 0.14 g g <sup>-1</sup>		

<sup>a</sup> RSE: relative standard error between predicted and experimental response. [\*] Solid-liquid ratio (SLR) of 1 : 25 g mL<sup>-1</sup> (intermediate value) was selected as the control, since no significant differences were observed in the hydration properties of untreated OP-DFC across the different SLR evaluated.



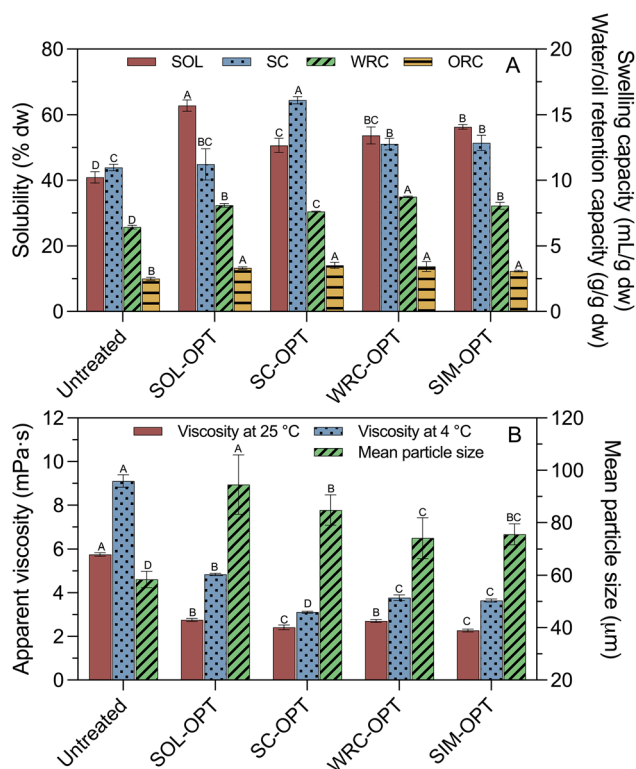


Fig. 1 (A) Techno-functional and (B) physical properties of orange peel dietary fibre concentrates under optimal ultrasound conditions for solubility (SOL), swelling capacity (SC), and water retention capacity (WRC), individually and simultaneously (SIM-OPT). Different letters indicate significant differences ( $p < 0.05$ ) within each property. SOL-OPT: 320 W, 1:30 SLR, 30 min; SC-OPT: 80 W, 1:25 SLR, 25.6 min; WRC-OPT: 208 W, 1:20 SLR, 30 min; SIM-OPT: 188 W, 1:28 SLR, 30 min.

SIM-OPT), lower SLR values resulted in higher SOL, supporting that US-induced disruption and release of soluble material are favoured in more diluted suspensions. These results differ from those reported in a recent study, which found no effect of US (400 W, 45 min, 1:37 SLR) on SOL in DFC obtained from orange pulp-peel mixtures.<sup>23</sup> Differences among studies suggest that, beyond certain thresholds of processing conditions, solubility of DFC derived from orange by-products may be hindered.

Swelling capacity increased by 50% under SC-OPT conditions and by 19% under both WRC-OPT and SIM-OPT treatments compared with untreated OP-DFC. Although SC values were relatively similar at intermediate-to-high powers (188–320 W), a clear downward trend was observed (188 > 208 > 320 W), with SOL-OPT ultimately showing no improvement over the control. These results are consistent with the regression model (3.1), where both power and treatment time had significant negative effects, and their interaction further accentuated the reduction in SC under prolonged high-power conditions. These results are consistent with previous studies on US-assisted extraction of pectin from grapefruit peel, where the highest SC of the resulting ingredient was achieved at power densities of 0.33–0.53 W mL<sup>-1</sup>.<sup>33</sup> In this context, the lowest power evaluated in the present study (80 W) corresponded to a power density of

0.4 W mL<sup>-1</sup> (~200 mL suspension), which falls within this optimal range.

Water retention capacity also improved under all conditions evaluated, with increases of 36% (WRC-OPT), 26% (SOL-OPT and SIM-OPT), and 19% (SC-OPT) compared to untreated OP-DFC. These results align with the regression model (3.1), which showed no significant effect of power, while treatment time exerted a positive influence, further enhanced by its interaction with SLR. Accordingly, the highest WRC was obtained under WRC-OPT (208 W, 1:20 SLR, 30 min), where the synergy between SLR and treatment time was maximised. In contrast, SC-OPT showed the lowest increase, as it was exposed to the shortest sonication treatment (25.6 min). Meanwhile, SOL-OPT (320 W, 30 min) and SIM-OPT (188 W, 30 min) resulted in similar WRC values despite their power differences, supporting that treatment time was a key factor influencing the WRC of OP-DFC. Similarly, Manthei *et al.*<sup>23</sup> reported an overall increase in WRC following US treatments, with no significant effect of US power. This enhancement has been attributed to the increased availability of hydrophilic functional groups resulting from cavitation-induced matrix disruption.<sup>23</sup>

The effect of US treatments on ORC, an indicator of the binding of lipids and lipid-soluble flavours during cooking, was also evaluated. Ultrasound treatments (307–1440 kJ kg<sup>-1</sup>) increased the ORC of OP-DFC by 23–41%, compared with the untreated counterpart; however, no significant ( $p > 0.05$ ) differences were observed among treatments (Fig. 1A). Recent studies applying US (~970–5800 kJ kg<sup>-1</sup>) on DFC derived from orange by-products found limited or no effects on ORC. A 7.6% increase was reported only under specific conditions (~1950 kJ kg<sup>-1</sup>, 400 W, 15 min, 1:37 SLR), whereas both higher and lower energy inputs showed no improvement compared to untreated DFC.<sup>16,23</sup> Differences across studies likely reflect variations in process severity. Under moderate US conditions, the DF matrix may loosen, creating pores that physically entrap lipids and expose internal hydrophobic groups, thereby enhancing lipid binding capacity.<sup>14,36</sup> Conversely, more intense conditions may cause structural collapse, diminishing potential gains in ORC.

**3.2.2. Physical properties.** Apparent viscosity was also evaluated as it influences the processability (*e.g.*, mixing, pumping, filling) and sensory attributes (*e.g.*, thickness, mouthfeel) of food products into which DF-rich ingredients are incorporated.<sup>37</sup> OP-DFC suspensions were prepared at a 6% (w/w) concentration, which complies with the “source of fibre” claim (>3% TDF dw) established by EFSA.<sup>25</sup> The apparent viscosity of untreated OP-DFC suspension was 5.76 mPa s at 25 °C and decreased by 52–61% in suspensions prepared with US-treated OP-DFC, with SOL-OPT and WRC-OPT exhibiting slightly higher values than SC-OPT and SIM-OPT (Fig. 1B). Ultrasound-induced decreases in viscosity have previously been reported as evidence of partial depolymerisation of plant cell walls.<sup>38</sup> This effect can be attributed to cavitation-induced mechanical forces acting at solid interfaces. These forces typically lead to particle fragmentation and weakened interparticle entanglements, ultimately lowering the viscosity of suspensions.<sup>15</sup> From a technological perspective, the reduced viscosity of 6% (w/w) OP-DFC suspensions offers promise for nutritional



improvement while limiting the viscosity increases usually associated with adding DF-rich ingredients into low-viscosity foods such as beverages and soups, which may contribute to preserving their original sensory attributes.

After 24 h at 4 °C, the apparent viscosity of untreated OP-DFC suspensions increased to 9.11 mPa s. This rise is likely due to the physical association of solubilised pectic substances during cold storage, promoting chain interactions and the formation of junction zones that immobilise water and thicken the suspension.<sup>39</sup> Similarly, all US-treated OP-DFC suspensions showed higher viscosities after cooling compared to 25 °C, yet they remained lower than that of the untreated OP-DFC suspension. Notably, the viscosity of the SOL-OPT suspension was 38% higher than that of suspensions obtained under the other US treatments (~3.5 mPa s). This trend likely reflects a greater release of soluble polysaccharides, including pectin, which thicken aqueous systems more effectively, particularly at low temperatures.<sup>40</sup>

The mean particle size of US-treated OP-DFC was 26–61% higher than that of the untreated counterpart (Fig. 1B). These results contrast with those reported by Manthei *et al.* (2024),<sup>23</sup> who reported particle size reduction of orange peel-pulp mixtures after US, although peel-rich formulations retained significantly larger particles than pulp-rich ones. During cavitation, soluble molecules such as proteins and polyphenols are released from citrus cells<sup>29</sup> and may interact with DF to form polysaccharide–protein and polysaccharide–polyphenol complexes,<sup>41,42</sup> thereby promoting agglomeration and increasing mean particle size. In agreement, a previous study by our group reported increased mean particle size of OP-DFC but decreased size in DFCs derived from orange bagasse following pulsed electric fields treatment.<sup>14</sup> This effect was suggested to arise from the significantly higher polyphenol content of the former. Despite the increase in particle size observed in the present study, the resulting values remained within the suggested range (~45–450 μm) to ensure adequate incorporation of DFCs into different food products.<sup>43</sup>

### 3.2.3. Total, insoluble, and soluble dietary fibre content.

Untreated OP-DFC consisted of 56.0% TDF, of which 49.4% corresponded to IDF and 6.6% to SDF. Following US treatments, IDF content decreased by 6.7–14.0%, while SDF levels increased by 44.0–83.6%, compared to untreated OP-DFC (Fig. 2). The most pronounced changes in DF fractions were observed under SOL-OPT conditions, where the IDF : SDF ratio decreased from 7.5 : 1 (untreated) to 3.5 : 1, followed by SIM-OPT (3.7 : 1), WRC-OPT (4.1 : 1), and SC-OPT (4.9 : 1). Only a slight decrease (0.7–3.7%) in TDF content was observed, suggesting that US treatments did not lead to major degradation of DF, but rather to a redistribution of their fractions. Furthermore, SDF content was strongly correlated with OP-DFC SOL ( $r = 0.9288$ ,  $p < 0.0001$ ), suggesting that US-driven gains in SOL likely arose from an increase in SDF. These results align with previous findings showing that US disrupts plant tissues and causes cell wall fragmentation, improving protopectin hydrolysis and pectin solubilisation in grapefruit peels.<sup>33</sup> In addition, US has been reported to promote partial depolymerisation of IDF into

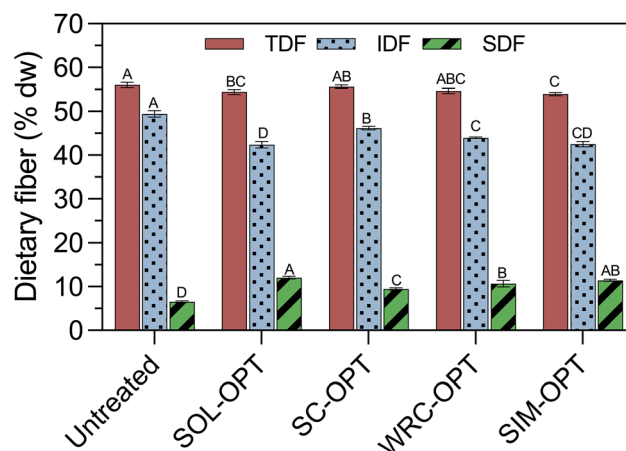


Fig. 2 Total (TDF), insoluble (IDF), and soluble dietary fibre (SDF) content in orange peel dietary fibre concentrates under optimal ultrasound conditions for solubility (SOL-OPT), swelling capacity (SC-OPT), and water retention capacity (WRC-OPT), individually and simultaneously (SIM-OPT). Different letters indicate significant differences ( $p < 0.05$ ) for each dietary fibre fraction. SOL-OPT: 320 W, 1 : 30 SLR, 30 min; SC-OPT: 80 W, 1 : 25 SLR, 25.6 min; WRC-OPT: 208 W, 1 : 20 SLR, 30 min; SIM-OPT: 188 W, 1 : 28 SLR, 30 min.

SDF in orange peel when combined with deep eutectic solvents.<sup>22</sup>

The higher SDF content observed in OP-DFC treated under SOL-OPT supports the apparent viscosity results (3.2.1), as it likely contributed to greater water immobilization during cold storage, resulting in the thickest suspension among US-treated systems.

**3.2.4. Microstructure.** The microstructure of untreated OP-DFC consisted of compact fragments with relatively smooth surfaces and few visible openings (Fig. 3A–C), in accordance with previous reports.<sup>14</sup> After US treatments, OP-DFC microstructure became rougher and more porous than that of the untreated material. These modifications are attributed to cavitation-induced shear forces causing tissue erosion and fragmentation.<sup>33,44</sup>

Among treatments, SOL-OPT induced the most pronounced structural changes in OP-DFC, transforming smooth surfaces into highly porous matrices that exposed internal structures (e.g., vascular bundles) (Fig. 3D–F). These features align with the intense treatment conditions applied ( $1440 \text{ kJ kg}^{-1}$ ), under which high power and prolonged sonication maximised matrix disruption. Moreover, the low SLR (1 : 30) results in a high energy input per unit of solid, further intensifying this effect. This degree of disruption is consistent with the release and solubilisation of cell wall polysaccharides, likely leading to the highest solubility (Fig. 1A) and SDF levels (Fig. 2). In addition, the more porous structure increases surface area, facilitating interactions between hydrophilic groups and water molecules and, in turn, contributing to the moderate enhancement in WRC (Fig. 1A).

In contrast, SC-OPT ( $307 \text{ kJ kg}^{-1}$ ) resulted in the least altered microstructure and was characterised by the presence of smooth and compact fragments, comparable to those in untreated OP-DFC, interspersed with rougher ones (Fig. 3G–I).



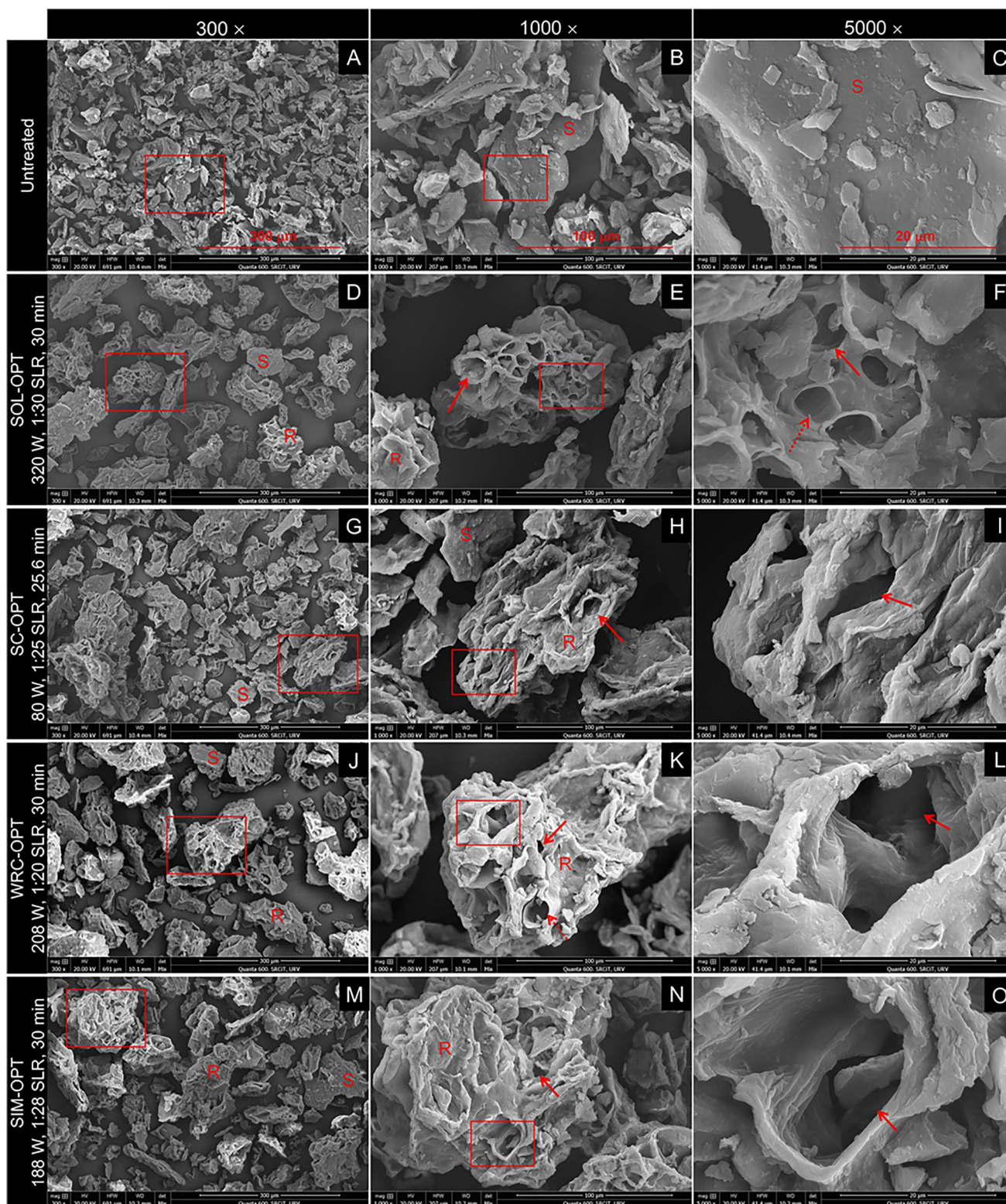


**Fig. 3** Scanning electron microscopy images of untreated orange peel dietary fibre concentrates (A–C) and concentrates treated under optimal ultrasound conditions for solubility (SOL-OPT, D–F), swelling capacity (SC-OPT, G–I), and water retention capacity (WRC-OPT, J–L), individually and simultaneously (SIM-OPT, M–O). Rectangles indicate the magnified areas, from left (300 $\times$ ) to right (5000 $\times$ ). Continuous arrows indicate pores; dotted arrows indicate exposure of internal structures; R: rough surface; S: smooth surface.



The latter exhibited irregular, folded surfaces with limited porosity. This loose yet not extensively disrupted morphology likely favoured water absorption within the DF network and subsequent expansion,<sup>17,34</sup> leading to the highest SC values among treatments (Fig. 1A). Unlike SOL-OPT OP-DFC, the absence of exposed vascular bundles supported a milder level of disruption. Accordingly, smaller increases in SOL, WRC, and SDF levels were observed under SC-OPT conditions (Fig. 1A and 2).

The microstructure of OP-DFC treated under WRC-OPT (Fig. 3J–L) was characterised by rough fragments with moderate porosity and limited exposure of internal structures, as fewer vascular bundles were observed compared with SOL-OPT. This structural configuration resulted in the highest WRC, possibly by providing sufficient exposure of hydrophilic groups while preserving matrix integrity, enabling efficient water binding and retention.<sup>17</sup> These features are consistent with the intermediate specific energy input applied ( $936 \text{ kJ kg}^{-1}$ ), which led to moderate increases in SOL, SC (Fig. 1A), and SDF levels (Fig. 2) compared with SOL-OPT and SC-OPT.

Orange peel-DFC treated under SIM-OPT (Fig. 3M–O) showed similar microstructural attributes to those observed following WRC-OPT, in agreement with the comparable energy input ( $846 \text{ kJ kg}^{-1}$ ). Accordingly, SOL and SC values were similar to those obtained under WRC-OPT. Nevertheless, WRC was lower under SIM-OPT (1 : 28 SLR) than WRC-OPT (1 : 20 SLR), likely due to the positive effect of higher solid concentrations on WRC, as previously discussed (3.1).

**3.2.5. Thermal properties.** The DSC thermogram of untreated OP-DFC showed a single endothermic event with peak temperature of  $163.5 \text{ }^\circ\text{C}$  (Fig. 4A), consistent with values previously reported for citrus by-products.<sup>14</sup> This transition has been attributed to water evaporation from heat absorption.<sup>45</sup>

The DSC profile of OP-DFC treated under SC-OPT ( $307 \text{ kJ kg}^{-1}$ ) was similar than that of the untreated counterpart, showing a small increase in peak temperature ( $+1.6 \text{ }^\circ\text{C}$ ) and associated enthalpy. These changes likely reflect the limited structural disruption induced by SC-OPT treatment (Fig. 3), which slightly loosens the matrix and promotes water absorption. In contrast, endothermic peak temperatures decreased by 7, 12, and  $28 \text{ }^\circ\text{C}$  for OP-DFC treated under WRC-OPT ( $936 \text{ kJ kg}^{-1}$ ), SIM-OPT ( $846 \text{ kJ kg}^{-1}$ ), and SOL-OPT ( $1440 \text{ kJ kg}^{-1}$ ) conditions, respectively, compared with untreated OP-DFC. These peaks were also broader and flatter, in line with a more heterogeneous matrix,<sup>46</sup> which required less energy for water release. This reduced thermal stability provides evidence for US-induced partial depolymerisation of DF and exposure of soluble domains in OP-DFC. The most pronounced changes occurred under SOL-OPT, reflecting its highly disrupted microstructure and increased pore density, where water molecules might interact weakly with the DF network. WRC-OPT and SIM-OPT showed intermediate decreases in peak temperature, in line with their moderate but evident matrix opening.

**3.2.6. Crystalline structural properties.** The diffractograms of untreated OP-DFC revealed low crystallinity, with a broad amorphous region centred between  $18\text{--}24^\circ 2\theta$ , characteristic of the disordered domains of pectin, hemicellulose, and

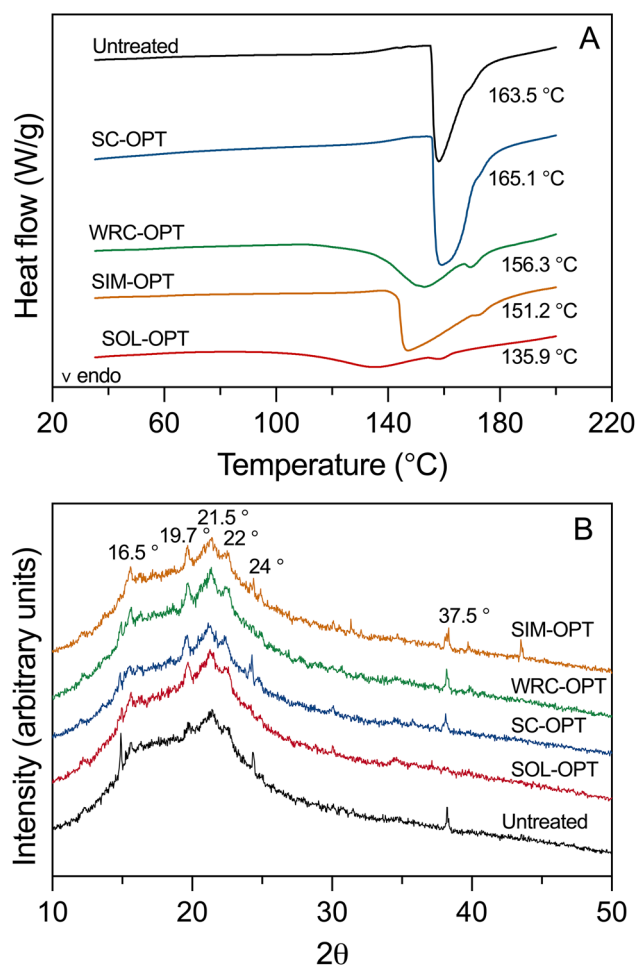


Fig. 4 (A) Differential scanning calorimetry thermograms and (B) X-ray diffraction patterns of orange peel dietary fibre concentrates under optimal ultrasound conditions for solubility (SOL-OPT), swelling capacity (SC-OPT), and water retention capacity (WRC-OPT), individually and simultaneously (SIM-OPT). SOL-OPT:  $320 \text{ W}$ , 1 : 30 SLR, 30 min; SC-OPT:  $80 \text{ W}$ , 1 : 25 SLR, 25.6 min; WRC-OPT:  $208 \text{ W}$ , 1 : 20 SLR, 30 min; SIM-OPT:  $188 \text{ W}$ , 1 : 28 SLR, 30 min.

amorphous cellulose in citrus cell wall polysaccharides.<sup>7,19,30</sup> Moreover, weak peaks at  $\sim 16.5^\circ$ ,  $21\text{--}22^\circ$ , and  $37.5^\circ 2\theta$  (Fig. 4B) appeared superimposed to this region, and were assigned to the crystalline cellulose I reflections from the 101, 002, and 004 planes, respectively.<sup>7,22</sup>

After US treatments, the positions of the cellulose diffraction peaks remained mostly unchanged, indicating that US treatments did not alter the crystalline structure of cellulose. However, the peaks in the  $18\text{--}22^\circ 2\theta$  region became slightly sharper than in untreated OP-DFC, suggesting an apparent increase in relative crystallinity. These results may reflect partial detachment of amorphous polymers, such as pectin, hemicellulose, and amorphous cellulose, from the cell wall matrix under US. This hypothesis is consistent with the redistribution of DF fractions and the increase in SDF content in OP-DFC (Fig. 2). Furthermore, under SOL-OPT conditions, the diffraction peak at  $37.5^\circ 2\theta$  disappeared, suggesting that the most intense US treatment ( $1440 \text{ kJ kg}^{-1}$ ) disrupted, at least partially,



the intra- and intermolecular hydrogen bonds responsible for conferring structural order to crystalline cellulose. This result aligns with DSC and SEM findings, where OP-DFC treated under SOL-OPT displayed the lowest thermal stability (Fig. 4A) and the greatest microstructural disruption (Fig. 3D–F).

**3.2.7. Molecular structure.** The normalized FTIR spectrum of untreated OP-DFC exhibited the characteristic absorption bands previously reported for cell wall polysaccharides in orange peel.<sup>14</sup> The spectra of US-treated OP-DFC showed the same band positions as the untreated counterpart, with small differences in peak relative intensities (Fig. 5).

The broad band at  $\sim 3330\text{ cm}^{-1}$  is assigned to O–H stretching vibrations  $\nu(\text{O–H})$ .<sup>47</sup> The  $\nu(\text{O–H})$  band intensity for OP-DFC treated under SC-OPT was comparable to that of untreated OP-DFC, whereas an increasing trend was observed for WRC-OPT (+1.4%), SIM-OPT (+7.4%), and SOL-OPT (+12.5%). This increase indicates greater availability of hydroxyl groups,<sup>45</sup> which overall tended to increase as the US energy input increased. These results are consistent with the cavitation-driven fragmentation of cell walls and pore formation (Fig. 3), that likely increases the exposure of hydroxyl groups previously involved in intra- or intermolecular interactions within the DF

network. The small increase in  $\nu(\text{O–H})$  band intensity of WRC-OPT likely reflects a balance between increased exposure of hydroxyl groups and higher levels of bound water, which is consistent with its highest WRC.

The band at  $\sim 2920\text{ cm}^{-1}$ , assigned to C–H stretching vibrations of methyl  $\nu(\text{CH}_2)$  and methylene  $\nu(\text{CH}_3)$  groups,<sup>47</sup> was used for spectral normalization, and remained unchanged in both untreated and US-treated spectra. The bands at  $\sim 1740$  and  $\sim 1605\text{ cm}^{-1}$  correspond to ester carbonyl stretching vibrations  $\nu(\text{C=O})$  and carboxylate antisymmetric stretching vibrations  $\nu(\text{COO}^-)$ , respectively.<sup>47</sup> After US treatments, the  $\nu(\text{C=O})$  band intensity decreased by  $\sim 15\%$  in all OP-DFC samples, consistent with partial pectin de-esterification caused by US-induced hydrolysis of methyl and acetyl groups.<sup>27,48</sup> Conversely, all US treatments led to increases in  $\nu(\text{COO}^-)$  band intensity. The largest rise (+25%) was observed under SOL-OPT conditions, reflecting more extensive DF network disruption and consequent exposure of hydrophilic groups. These results support the enhanced hydration properties of US-treated OP-DFC, as newly available carboxyl groups can bind water molecules through electrostatic and hydrogen bond interactions, thus enhancing SOL, SC, and WRC.

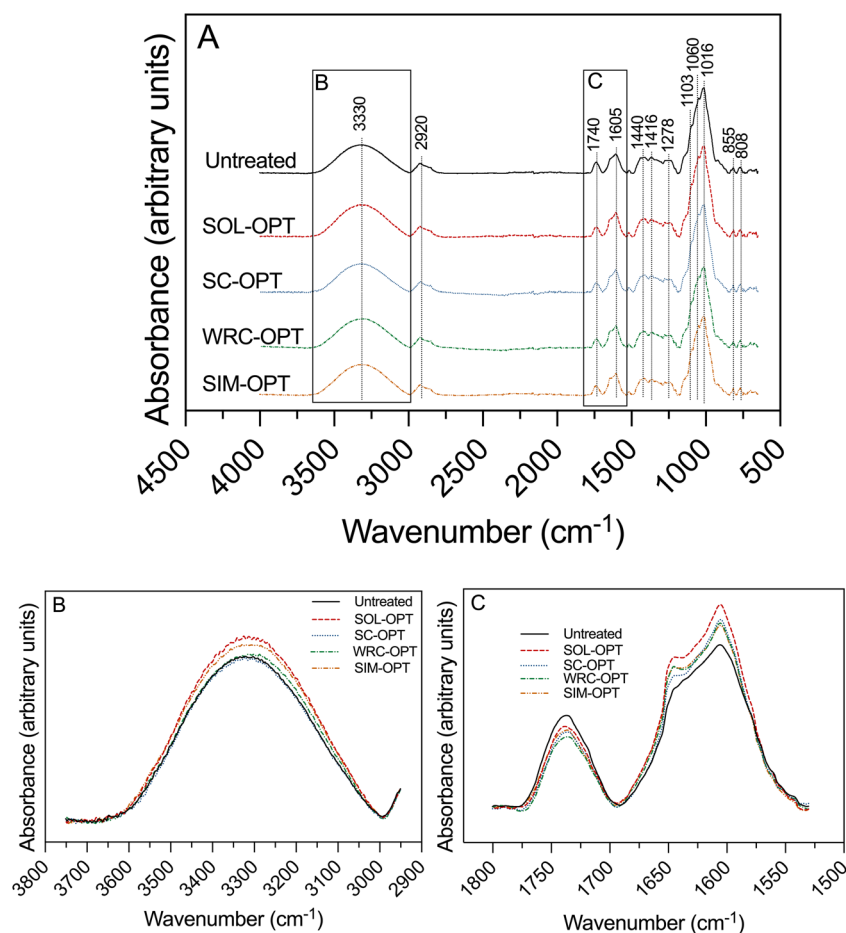


Fig. 5 FTIR spectra of orange peel dietary fibre concentrates under optimal ultrasound conditions for solubility (SOL-OPT), swelling capacity (SC-OPT), and water retention capacity (WRC-OPT), individually and simultaneously (SIM-OPT). (A) full FTIR spectra; (B) magnified region from 3800 to 2900  $\text{cm}^{-1}$ ; (C) magnified region from 1800 to 1500  $\text{cm}^{-1}$ . SOL-OPT: 320 W, 1:30 SLR, 30 min; SC-OPT: 80 W, 1:25 SLR, 25.6 min; WRC-OPT: 208 W, 1:20 SLR, 30 min; SIM-OPT: 188 W, 1:28 SLR, 30 min.



The absorption bands at  $\sim 1440$  and  $\sim 1416$   $\text{cm}^{-1}$  arise from  $\text{CH}_2$  bending  $\delta(\text{CH}_2)$  in cellulose and  $\nu(\text{COO}^-)$  symmetric stretching in pectin and xyloglucan (hemicellulose), respectively. The absorption band at  $\sim 1278$   $\text{cm}^{-1}$  is attributed to C–O stretching vibrations  $\nu(\text{C–O})$  of pectin. In addition, the region centred at  $\sim 1200$ – $900$   $\text{cm}^{-1}$  contained contributions from several bond vibrations, including  $\nu(\text{C–O})$  and  $\nu(\text{C–C})$  of the polysaccharide backbone of cellulose ( $\sim 1101$  and  $\sim 1030$   $\text{cm}^{-1}$ ), pectin ( $\sim 1093$  and  $\sim 1014$   $\text{cm}^{-1}$ ), and xyloglucan ( $\sim 1071$   $\text{cm}^{-1}$ ). The bands at  $\sim 850$  and  $830$   $\text{cm}^{-1}$  are assigned to  $\text{C}_1\text{–H}$  bending in cellulose/xyloglucan, and ring vibration in pectin, respectively.<sup>49</sup> Overall, no major changes were observed in these band intensities across treatments. In particular, the comparable intensity of peaks in the  $1200$ – $900$   $\text{cm}^{-1}$  region between untreated and US-treated OP-DFC suggests that the glycosidic backbone of DF polysaccharides was largely preserved under the US conditions evaluated in this study. Instead, US likely promoted the detachment of smaller domains, held together by non-covalent interactions, and the partial de-esterification of pectin. These structural rearrangements are consistent with matrix loosening which the increased SDF content and exposed hydrophilic groups (hydroxyl and carboxyl), together contributing to the improved hydration properties.

## 4. Conclusions

This study demonstrated that RSM adequately modelled and quantified the effect of US treatment conditions (power, SLR, and time) on SOL, SC, and WRC of OP-DFC and reliably predicted the conditions that maximised these hydration properties. Relatively long US treatments (25.6–30 min) increased all hydration properties, whereas optimal US power and SLR combinations were  $320$  W –  $1 : 30$   $\text{g mL}^{-1}$  for SOL,  $80$  W –  $1 : 25$   $\text{g mL}^{-1}$  for SC, and  $208$  W –  $1 : 20$   $\text{g mL}^{-1}$  for WRC. Simultaneous optimisation yielded the best compromise at  $188$  W,  $1 : 28$   $\text{g mL}^{-1}$ , and  $30$  min of sonication. Enhancements in hydration properties were mechanistically associated with cavitation-induced DF matrix disruption, pore formation, redistribution of DF fractions, and the release of amorphous domains from the DF network. Notably, the glycosidic backbone of polysaccharides remained largely intact, with only partial depolymerisation occurring under US treatments, as supported by decreases in the apparent viscosity of OP-DFC suspensions. These physical modifications led to an increase in surface area, SDF levels, and exposure of hydrophilic groups, which in turn increased SOL, SC, and WRC. The extent of these effects depended on treatment conditions. Higher powers and lower SLRs produced greater structural disruption and higher SDF levels, increasing SOL. From an industrial perspective, increasing SOL without introducing viscosity changes facilitates the incorporation of DF-rich ingredients into beverages and liquid foods, improving their nutritional profile while preserving desirable sensory attributes. Low-to-medium powers and medium-to-high SLRs better preserved the microstructure and promoted water absorption and capillary effects, enhancing SC and WRC. In this context, higher SC contributes to reducing lump formation during powder rehydration and supports

structure development in semi-solid systems, such as cake batters. Likewise, improved WRC enhances the binder performance of ingredients in food systems, which may contribute to increased juiciness in processed meats and meat analogues and to reduced moisture loss and staling in baked goods. Overall, US can be strategically applied to tailor the hydration properties of OP-DFC while contributing to the sustainable valorisation of underutilised orange peels through physical, water-based processes and supporting the development of clean-label, value-added ingredients within a circular bioeconomy framework.

## Author contributions

Julia Nutter: conceptualization, data curation, formal analysis, investigation, methodology, validation, visualization, writing – original manuscript. Robert Soliva-Fortuny: funding acquisition, writing – review and edition. Olga Martín-Belloso: writing – review and edition. Pedro Elez-Martínez: conceptualization, funding acquisition, project administration, supervision, visualization, writing – review, and edition.

## Conflicts of interest

There are no conflicts to declare.

## Data availability

The data that support the findings of this study are openly available in CORA – Repositori de Dades de Recerca at <https://doi.org/10.34810/data2794>.

Supplementary information (SI) is available. See DOI: <https://doi.org/10.1039/d5fb00922g>.

## Acknowledgements

The authors acknowledge the project RTI 2018-095560-B-I00 funded by MICIU/AEI/10.13039/501100011033/and by FEDER A way to make Europe and the project TED2021-131828B-I00 funded by MICIU/AEI/10.13039/501100011033 and by the European Union NextGenerationEU/PRTR.

## References

- 1 I. Valencia-Espinosa, J. Welti-Chanes, L. E. Garcia-Amezquita and V. Tejada-Ortigoza, Green extraction and modification of dietary fiber from traditional and novel sources, in *Sustainable Food Science: A Comprehensive Approach*, ed. P. Ferranti, Elsevier, Amsterdam, 1st edn, 2023, ch. 4.14, pp. 254–270, DOI: [10.1016/B978-0-12-823960-5.00081-0](https://doi.org/10.1016/B978-0-12-823960-5.00081-0).
- 2 T. M. Barber, S. Kabisch, A. F. H. Pfei and M. O. Weickert, The health benefits of dietary fibre, *Nutrients*, 2020, **12**(10), 1–17, DOI: [10.3390/nu12103209](https://doi.org/10.3390/nu12103209).
- 3 J. Y. Huang, J. S. Liao, J. R. Qi, W. X. Jiang and X. Yang, Structural and physicochemical properties of pectin-rich dietary fiber prepared from citrus peel, *Food Hydrocolloids*, 2021, **110**, 106140, DOI: [10.1016/j.foodhyd.2020.106140](https://doi.org/10.1016/j.foodhyd.2020.106140).



- 4 R. Tolve, M. Zaroni, G. Ferrentino, R. Gonzalez-Ortega, L. Sportiello, M. Scampicchio and F. Favati, Dietary fibers effects on physical, thermal, and sensory properties of low-fat ice cream, *LWT-Food Sci. Technol.*, 2024, **199**, 116094, DOI: [10.1016/j.lwt.2024.116094](https://doi.org/10.1016/j.lwt.2024.116094).
- 5 S. Arapi, A. T. Pamase, B. De Meulenaer and P. Van der Meeren, The effect of protein-pectin interactions on the functional properties of soy drinks in coffee applications, *Food Hydrocolloids*, 2025, **168**, 111487, DOI: [10.1016/j.foodhyd.2025.111487](https://doi.org/10.1016/j.foodhyd.2025.111487).
- 6 J. Sang, L. Li, J. Wen, Q. Gu, J. Wu, Y. Yu, Y. Xu, M. Fu and X. Lin, Evaluation of the structural, physicochemical and functional properties of dietary fiber extracted from Newhall navel orange by-products, *Foods*, 2021, **10**, 12772, DOI: [10.3390/foods10112772](https://doi.org/10.3390/foods10112772).
- 7 A. Scurria, L. Albanese, M. Pagliaro, F. Zabini, F. Giordano, F. Meneguzzo and R. Ciriminna, CytoCell: Valued cellulose from citrus processing waste, *Molecules*, 2021, **26**(3), 596, DOI: [10.3390/molecules26030596](https://doi.org/10.3390/molecules26030596).
- 8 C. E. Wagner and G. M. Ganjyal, Impact of functional dietary fiber incorporation on the appearance and mechanical properties of extruded high moisture meat analogs, *J. Food Sci.*, 2024, **89**, 4953–4968, DOI: [10.1111/1750-3841.17164](https://doi.org/10.1111/1750-3841.17164).
- 9 A. Marczak and A. C. Mendes, Dietary fibers: Shaping textural and functional properties of processed meats and plant-based meat alternatives, *Foods*, 2024, **13**(12), 1952, DOI: [10.3390/foods13121952](https://doi.org/10.3390/foods13121952).
- 10 C. Verbeke, E. Debonne, S. Versele, F. Van Bockstaele and M. Eeckhout, Technological evaluation of fiber effects in wheat-based dough and bread, *Foods*, 2024, **13**(16), 1–16, DOI: [10.3390/foods13162582](https://doi.org/10.3390/foods13162582).
- 11 A. Aydogdu, G. Sumnu and S. Sahin, Effects of addition of different fibers on rheological characteristics of cake batter and quality of cakes, *J. Food Sci. Technol.*, 2018, **55**, 667–677, DOI: [10.1007/s13197-017-2976-y](https://doi.org/10.1007/s13197-017-2976-y).
- 12 Y. Wang, X. Wang, M. Li, L. Li and S. Ma, Effect of wheat bran dietary fiber on yeast, sourdough and *Lactobacillus plantarum* fermented dough: insight from gluten protein structure and aggregation behavior, *Food Chem.*, 2026, **501**, 147574, DOI: [10.1016/j.foodchem.2025.147574](https://doi.org/10.1016/j.foodchem.2025.147574).
- 13 A. Díaz-Núñez, G. López-Gámez, O. Martín-Belloso, R. Soliva-Fortuny and P. Elez-Martínez, Optimizing enzymatic processing of apple pomace: A strategy for modifying techno-functional properties and dietary fiber, *Eur. Food Res. Technol.*, 2025, **251**, 4589–4603, DOI: [10.1007/s00217-025-04888-7](https://doi.org/10.1007/s00217-025-04888-7).
- 14 J. Nutter, R. Soliva-Fortuny, O. Martín-Belloso and P. Elez-Martínez, Pulsed electric fields technology enhances the functionality of orange by-products: A study on dietary fiber fractions and structure, *Innovative Food Sci. Emerging Technol.*, 2025, **104**, 104100, DOI: [10.1016/j.ifset.2025.104100](https://doi.org/10.1016/j.ifset.2025.104100).
- 15 K. C. Martinez-Solano, N. A. Garcia-Carrera, V. Tejada-Ortigoza, T. García-Cayuela and L. E. Garcia-Amezquita, Ultrasound extraction and modification of fiber-rich by-products, *Food Eng. Rev.*, 2021, **13**, 524–543, DOI: [10.1007/s12393-020-09269-2](https://doi.org/10.1007/s12393-020-09269-2).
- 16 A. Manthei, P. Elez-Martínez, R. Soliva-Fortuny and P. Murciano-Martínez, Ultrasonication and enzymatic treatment of apple and orange bagasses: Molecular characterization of released oligosaccharides and modification of techno-functional and health-related properties, *LWT-Food Sci. Technol.*, 2024, **194**, 115816, DOI: [10.1016/j.lwt.2024.115816](https://doi.org/10.1016/j.lwt.2024.115816).
- 17 L. Huang, X. Ding, Y. Zhao, Y. Li and H. Ma, Modification of insoluble dietary fiber from garlic straw with ultrasonic treatment, *J. Food Process. Preserv.*, 2018, **42**, 13399, DOI: [10.1111/jfpp.13399](https://doi.org/10.1111/jfpp.13399).
- 18 X. Zhu, R. S. Das, M. L. Bhavya, M. Garcia-Vaquero and B. K. Tiwari, Acoustic cavitation for agri-food applications: Mechanism of action, design of new systems, challenges and strategies for scale-up, *Ultrason. Sonochem.*, 2024, **105**, 106850, DOI: [10.1016/j.ultsonch.2024.106850](https://doi.org/10.1016/j.ultsonch.2024.106850).
- 19 J. Chu, P. Metcalfe, H. V. Linford, S. Zho, F. M. Goycoolea, S. Chen, X. Ye, M. Holmes and C. Orfila, Short-time acoustic and hydrodynamic cavitation improves dispersibility and functionality of pectin-rich biopolymers from citrus waste, 2022, **330**, 129789, DOI: [10.1016/j.jclepro.2021.129789](https://doi.org/10.1016/j.jclepro.2021.129789).
- 20 D. Panwar, P. S. Panesar and H. K. Chopra, Green extraction of pectin from *Citrus limetta* peels using organic acid and its characterization, *Biomass Convers. Biorefin.*, 2021, **14**, 159–171, DOI: [10.1007/s13399-021-02127-z](https://doi.org/10.1007/s13399-021-02127-z).
- 21 W. Wang, Y. Feng, W. Chen, K. Adie, D. Liu and Y. Yin, Citrus pectin modified by microfluidization and ultrasonication: Improved emulsifying and encapsulation properties, *Ultrason. Sonochem.*, 2021, **70**, 105322, DOI: [10.1016/j.ultsonch.2020.105322](https://doi.org/10.1016/j.ultsonch.2020.105322).
- 22 L. Zhou, J. Luo, Q. Xie, L. Huang, D. Shen and G. Li, Dietary fiber from navel orange peel prepared by enzymatic and ultrasound-assisted deep eutectic solvents: Physicochemical and prebiotic properties, *Foods*, 2023, **12**, 104100, DOI: [10.3390/foods12102007](https://doi.org/10.3390/foods12102007).
- 23 A. Manthei, P. Elez-Martínez, O. Martín-Belloso and R. Soliva-Fortuny, Modification of techno-functional and health-promoting properties of orange by-products through ultrasonication, *Sustainable Food Technol.*, 2024, **2**(6), 1757–1769, DOI: [10.1039/d4fb00215f](https://doi.org/10.1039/d4fb00215f).
- 24 M. B. Bengardino, M. V. Fernandez, J. Nutter, R. J. Jagus and M. V. Agüero, Recovery of bioactive compounds from beet leavesthrough simultaneous extraction: Modelling and process optimization, *Food Bioprod. Process.*, 2019, **118**, 227–236, DOI: [10.1016/j.fbp.2019.09.013](https://doi.org/10.1016/j.fbp.2019.09.013).
- 25 European Safety Authority, Scientific opinion on dietary fibre health claims, *EFSA J.*, 2010, **8**, 1735, DOI: [10.2903/j.efsa.2010.1735](https://doi.org/10.2903/j.efsa.2010.1735).
- 26 I. Goñi, M. E. Díaz-Rubio, J. Pérez-Jiménez and F. Saura-Calixto, Towards an updated methodology for measurement of dietary fiber, including associated polyphenols, in food and beverages, *Food Res. Int.*, 2009, **42**(7), 840–846, DOI: [10.1016/j.foodres.2009.03.010](https://doi.org/10.1016/j.foodres.2009.03.010).
- 27 M. J. Baker, J. Trevisan, P. Bassan, R. Bhargava, H. J. Butler, K. M. Dorling, P. R. Fielden, S. W. Fogarty, N. J. Fullwood, K. a Heys, C. Hughes, P. Lasch, P. L. Martin-Hirsch,



- B. Obinaju, G. D. Sockalingum, J. Sulé-Suso, R. J. Strong, M. J. Walsh, B. R. Wood, P. Gardner and F. L. Martin, Using Fourier transform IR spectroscopy to analyze biological materials, *Nat. Protoc.*, 2014, **9**(8), 1771–1791, DOI: [10.1038/nprot.2014.110](https://doi.org/10.1038/nprot.2014.110).
- 28 C. Freitas de Oliveira, D. Giordani, R. Lutckemier, P. D. Gurak, F. Cladera-Olivera and L. D. Ferreira Marczak, Extraction of pectin from passion fruit peel assisted by ultrasound, *LWT–Food Sci. Technol.*, 2016, **71**, 110–115, DOI: [10.1016/j.lwt.2016.03.027](https://doi.org/10.1016/j.lwt.2016.03.027).
- 29 M. D. C. Razola-Díaz, E. J. Guerra-Hernández, C. Rodríguez-Pérez, A. M. Gómez-Caravaca, B. García-Villanova and V. Verardo, Optimization of ultrasound-assisted extraction via sonotrode of phenolic compounds from orange by-products, *Foods*, 2021, **10**, 1120, DOI: [10.3390/foods10051120](https://doi.org/10.3390/foods10051120).
- 30 I. M. Savic, I. M. Savic Gajic, M. G. Milovanovic, S. Zerajic and D. Gajic, Optimization of ultrasound-assisted extraction and encapsulation of antioxidants from orange peels in alginate-chitosan microparticles, *Antioxidants*, 2022, **11**(2), 297, DOI: [10.3390/antiox11020297](https://doi.org/10.3390/antiox11020297).
- 31 R. Cui and F. Zhu, Ultrasound modified polysaccharides: A review of structure, physicochemical properties, biological activities and food applications, *Trends Food Sci. Technol.*, 2021, **107**, 491–508, DOI: [10.1016/j.tifs.2020.11.018](https://doi.org/10.1016/j.tifs.2020.11.018).
- 32 R. Minjares-Fuentes, A. Femenia, M. C. Garau, M. G. Candelas-Cadillo, S. Simal and C. Rosselló, Ultrasound-assisted extraction of hemicelluloses from grape pomace using response surface methodology, *Carbohydr. Polym.*, 2016, **138**, 180–191, DOI: [10.1016/j.carbpol.2015.11.045](https://doi.org/10.1016/j.carbpol.2015.11.045).
- 33 Y. Xu, L. Zhang, Y. Bailina, Z. Ge, T. Ding, X. Ye and D. Liu, Effects of ultrasound and/or heating on the extraction of pectin from grapefruit peel, *J. Food Eng.*, 2014, **126**, 72–81, DOI: [10.1016/j.jfoodeng.2013.11.004](https://doi.org/10.1016/j.jfoodeng.2013.11.004).
- 34 J. Yan, S. Jiang, Q. Wang, O. Dai, Z. Yang, B. Huang, R. Huang, Z. Chi, Y. Sun and J. Pang, The effects of ultrasound on the rehydration of konjac glucomannan/soy protein isolate gel and simulation of gas-liquid interface evolution during the rehydration process, *Foods*, 2024, **13**, 4136, DOI: [10.3390/foods13244136](https://doi.org/10.3390/foods13244136).
- 35 X. Fan, H. Chang, Y. Ling, X. Zhao, A. Zhang, S. Li and Z. Feng, Effects of ultrasound-assisted enzyme hydrolysis on the microstructure and physicochemical properties of okara fibers, *Ultrason. Sonochem.*, 2020, **69**, 105247, DOI: [10.1016/j.ultsonch.2020.105247](https://doi.org/10.1016/j.ultsonch.2020.105247).
- 36 S. Li, N. Hu, J. Zhu, M. Zheng, H. Liu and J. Liu, Influence of modification methods on physicochemical and structural properties of soluble dietary fiber from corn bran, *Food Chem. X*, 2022, **14**, 100298, DOI: [10.1016/j.fochx.2022.100298](https://doi.org/10.1016/j.fochx.2022.100298).
- 37 A. Deblais, E. den Hollander, C. Boucon, A. E. Blok, B. Veltkamp, P. Voudouris, P. Versluis, H.-J. Kim, M. Mellema, M. Stieger, D. Bonn and K. P. Velikov, Predicting thickness perception of liquid food products from their non-Newtonian rheology, *Nat. Commun.*, 2021, **12**, 26687, DOI: [10.1038/s41467-021-26687-w](https://doi.org/10.1038/s41467-021-26687-w).
- 38 J. Li, B. Li, P. Geng, A. X. Song and J. Y. Wu, Ultrasonic degradation of konjac glucomannan and the effect of freezing combined with alkali treatment on their rheological profiles, *Food Hydrocolloids*, 2017, **70**, 14–19, DOI: [10.3390/molecules24101860](https://doi.org/10.3390/molecules24101860).
- 39 U. Einhorn-Stoll, Pectin-water interactions in foods – From powder to gel, *Food Hydrocolloids*, 2018, **78**, 109–119, DOI: [10.1016/j.foodhyd.2017.05.029](https://doi.org/10.1016/j.foodhyd.2017.05.029).
- 40 D. Gawkowska, J. Cybulska and A. Zdunek, Structure-related gelling of pectins and linking with other natural compounds: a review, *Polymers*, 2018, **10**(7), 762, DOI: [10.3390/polym10070762](https://doi.org/10.3390/polym10070762).
- 41 A. Fernandes, N. Mateus and V. de Freitas, Polyphenol-dietary fiber conjugates from fruits and vegetables: nature and biological fate in a food and nutrition perspective, *Foods*, 2023, **12**(5), 1052, DOI: [10.3390/foods12051052](https://doi.org/10.3390/foods12051052).
- 42 A. Siemińska-Kuczer, M. Szymańska-Chargot and A. Zdunek, Recent advances in interactions between polyphenols and plant cell wall polysaccharides as studied using an adsorption technique, *Food Chem.*, 2022, **373**(B), 131487, DOI: [10.1016/j.foodchem.2021.131487](https://doi.org/10.1016/j.foodchem.2021.131487).
- 43 L. E. Garcia-Amezquita, V. Tejada-Ortigoza, S. O. Serna-Saldivar and J. Welte-Chanes, Dietary fiber concentrates from fruit and vegetable by-products: Processing, modification, and application as functional ingredients, *Food Bioprocess Technol.*, 2018, **11**, 1439–1463, DOI: [10.1007/s11947-018-2117-2](https://doi.org/10.1007/s11947-018-2117-2).
- 44 Z. Dou, C. Chen and X. Fu, The effect of ultrasound irradiation on the physicochemical properties and  $\alpha$ -glucosidase inhibitory effect of blackberry fruit polysaccharide, *Food Hydrocolloids*, 2019, **96**, 568–576, DOI: [10.1016/j.foodhyd.2019.06.002](https://doi.org/10.1016/j.foodhyd.2019.06.002).
- 45 H. Ouyang, B. Guo, Y. Hu, L. Li, Z. Jiang, Q. Li, H. Ni, Z. Li and M. Zheng, Effect of ultra-high-pressure treatment on structural and functional properties of dietary fiber from pomelo fruitlets, *Food Biosci.*, 2023, **52**, 102436, DOI: [10.1016/j.fbio.2023.102436](https://doi.org/10.1016/j.fbio.2023.102436).
- 46 U. Einhorn-Stoll, H. Kastner and S. Drusch, Thermally induced degradation of citrus pectins during storage – Alterations in molecular structure, colour and thermal analysis, *Food Hydrocolloids*, 2014, **35**, 565–575, DOI: [10.1016/j.foodhyd.2013.07.020](https://doi.org/10.1016/j.foodhyd.2013.07.020).
- 47 B. Gieroba, G. Kalisz, M. Krysa, M. Khalavka and A. Przekora, Application of vibrational spectroscopic techniques in the study of the natural polysaccharides and their cross-linking process, *Int. J. Mol. Sci.*, 2023, **24**(3), 2630, DOI: [10.3390/ijms24032630](https://doi.org/10.3390/ijms24032630).
- 48 H. Bagherian, F. Zokaee Ashtiani, A. Fouladitajar and M. Mohtashamy, Comparisons between conventional, microwave- and ultrasound-assisted methods for extraction of pectin from grapefruit, *Chem. Eng. Process.*, 2011, **50**(11–12), 1237–1243, DOI: [10.1016/j.cep.2011.08.002](https://doi.org/10.1016/j.cep.2011.08.002).
- 49 M. Szymanska-Chargot and A. Zdunek, Use of FT-IR Spectra and PCA to the bulk characterization of cell wall residues of fruits and vegetables along a fraction process, *Food Biophys.*, 2013, **8**(1), 29–42, DOI: [10.1007/s11483-012-9279-7](https://doi.org/10.1007/s11483-012-9279-7).

